JCTC Journal of Chemical Theory and Computation

Article

pubs.acs.org/JCTC

Extension of the AMBER Force Field for Nitroxide Radicals and Combined QM/MM/PCM Approach to the Accurate Determination of EPR Parameters of DMPO-H in Solution

Laura Hermosilla,*[,†] Giacomo Prampolini,*[,‡] Paloma Calle,[†] José Manuel García de la Vega,[†] Giuseppe Brancato,[§] and Vincenzo Barone[§]

[†]Departamento de Química Física Aplicada, Facultad de Ciencias, Universidad Autónoma de Madrid, 28049 Madrid, Spain

[‡]Istituto per i Processi Chimico-Fisici, Consiglio Nazionale delle Ricerche, Area della Ricerca, via Moruzzi 1, I-56124 Pisa, Italy

[§]Scuola Normale Superiore, Piazza dei Cavalieri 7, I-56126 Pisa, Italy

Supporting Information

ABSTRACT: A computational strategy that combines both time-dependent and time-independent approaches is exploited to accurately model molecular dynamics and solvent effects on the isotropic hyperfine coupling constants of the DMPO-H nitroxide. Our recent general force field for nitroxides derived from AMBER ff99SB is further extended to systems involving hydrogen atoms in β-positions with respect to NO-moiety. The resulting force-field has been employed in a series of classical molecular dynamics simulations, comparing the computed EPR parameters from selected molecular configurations to the corresponding experimental data in different solvents. The effect of vibrational averaging on the spectroscopic parameters is also taken into account, by second-order vibrational perturbation theory involving semidiagonal third energy derivatives together first and second property derivatives.

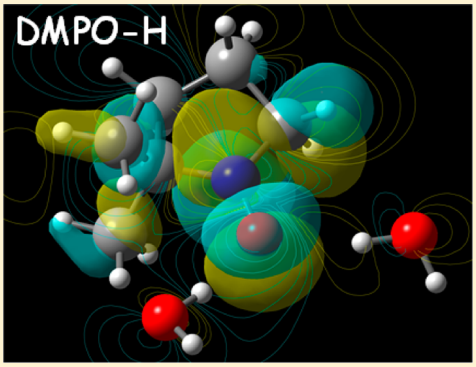

1. INTRODUCTION

Free radicals are of remarkable interest in chemistry, biology, biophysics, and medicine because they are involved in many different features of metabolism.[1,2] Electron Paramagnetic Resonance (EPR) spectroscopy is a specific technique for the detection of free radicals. Unfortunately, it is not always possible to observe directly free radicals, as their concentration may be below the detection limit and/or their spin relaxation times may be very short at physiological temperature. Spin trapping provides a way to overcome these problems, since it implies the addition of the free radical of interest to a diamagnetic compound, spin trap, to form a relatively long-lived free radical product, spin adduct, which conceivably accumulates to a concentration high enough to be detected by EPR. The information about the radical trapped is contained in the hyperfine splitting of the spin adducts. Therefore, the analysis of the resulting EPR spectrum allows the identification of the original radical or, at least, the extraction of valuable information about its nature.

Spin adducts are usually nitroxides and are relatively stable thanks to the resonance stabilization of the unpaired electron.[3] 5,5-Dimethylpyrroline-1-oxide, DMPO, which is one of the most used spin traps, adds the trapped radical to the carbon adjacent to the nitrogen, Figure 1, so that the splittings due to both the nitrogen and the β-hydrogen can provide considerable information about the trapped radical. Such splittings, especially the isotropic hyperfine coupling constants, are obviously influenced by the nature of the trapped radical, but also the solvent can have a significant effect on such parameters; in general, an increase in solvent polarity produces larger nitrogen hyperfine coupling constants, as the spin density on the nitrogen augments.[4] Therefore, the reliable determination of the hyperfine coupling constants of both the nitrogen and the β-hydrogen of the DMPO-R radical adduct is of fundamental importance to correctly interpret the experimental results.

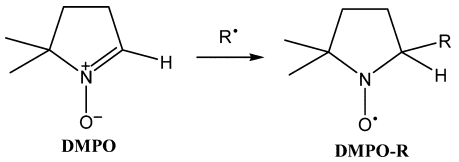

Figure 1. Spin trapping of free radical R by DMPO spin trap to form DMPO-R adduct.

The chemical stability of the nitroxide moiety under ordinary conditions,[3] coupled with the high sensitivity of some magnetic properties toward interactions with its surrounding, make possible to investigate several physical−chemical processes involving this kind of molecules.[1,2,5,6] Modern spectroscopic techniques like high-field EPR and ENDOR provide a wealth of information, which is encoded essentially in the hyperfine coupling (a) and gyromagnetic (g) tensors.[7] Unfortunately, the

Received: April 19, 2013
Published: June 25, 2013

relationship between the observed spectroscopic features and the underlying structural/dynamic behavior is only indirect, and the interpretation of experimental results is not without ambiguities, especially when different (intrinsic and environmental) effects contribute to the overall observables. In this framework, theoretical approaches are becoming important and versatile tools for the assignment and interpretation of experimental spectra. In particular, synergic strategies that combine experimental measurements and theoretical calculations can give a better understanding of the interplay between magnetic and structural/dynamic properties of complex systems.[8]

Interpretation of the experiments in structural terms strongly benefits from quantum mechanical (QM) calculations able to dissect the overall observables in several distinct subtle effects.[9−11] In particular, many studies have been devoted to the comparison between experimental and computed EPR properties of both aliphatic and aromatic nitroxides.[9−24] Despite the large difference in the flexibility of the ring structure that is expected between these two classes, it has been shown[22,23,25−27] that vibrational averaging effects should be taken into account for a correct interpretation of the experimental results not only for aliphatic but also for aromatic nitroxides. Indeed, several papers have examined in detail the main effects influencing the magnetic parameters of nitroxides, such as geometry around the NO moiety, electron donating propensity of the substituents, polarity and hydrogen-bonding power of the embedding medium, and inversion motion at the nitrogen atom.[9] Recently, a general computational strategy, rooted into density functional theory (DFT),[10,17] has been proposed for the analysis of spin probing experiments, with the aim of providing an accurate description of the thermodynamic and spectroscopic properties of several nitroxides.[18,22,23,27] Specifically, it has been shown that the PBE0/N07D computational model provides remarkably accurate structural, vibrational, and magnetic parameters.[28−34] In addition, the reliability of the PBE0 functional for describing intermolecular interactions involving nitroxides and water molecules has been confirmed as well.[35]

Concerning solvent effects, an effective computational methodology is to adopt the well-known Polarizable Continuum Model (PCM).[36,37] Nevertheless, when highly specific solute−solvent interactions (e.g., H-bonding) are thought to play a relevant role, both solute and (at least) the closest solvent molecules should be included within the explicit quantum-mechanical system, maintaining the PCM to account for bulk solvent effects.[38−45] This procedure, often referred to as the cluster−PCM approach, is also attractive for the computation of averaging effects brought about by dynamics.

From a computational point of view, the problem of accurately reproducing spectroscopic parameters of molecules in solution and accounting for dynamical effects can be addressed by adopting a time-dependent protocol, based on sampling a representative region of the configuration space of the solute/solvent system, populated during the system dynamics, and then retrieving the physical−chemical observables from statistical averages. Born−Oppenheimer dynamics and, more importantly, extended Lagrangian approaches like the Car−Parrinello prototype[46] have been adopted to provide dynamical trajectories long enough to allow for reasonable averaging of spectroscopic parameters of small size nitroxide free radicals.[45,47−49] However, computational simulations of large nitroxide systems in gas and in condensed phases can hardly rely on sophisticated QM methods alone.

From another point of view, vibrational averaging of spectroscopic observables and characterization of the conformational changes and of the dynamical behavior of such systems require long simulation times. In these cases, a more efficient and feasible strategy is provided by the development of integrated computational approaches that combine DFT with less expensive molecular mechanics/molecular dynamics (MM/MD) methods capable of describing larger molecular systems and longer MD trajectories than those accessible by QM models. However, this approach rests on the availability of simple and accurate force-fields (FFs) for the description of potential energy surfaces (PES) governing both intra- and intermolecular interactions. While the combined use of experimental and QM reference data has been particularly useful in the fitting of parameters,[50] an attractive alternative is to derive FFs that attempt to reproduce the results of QM methods alone.[51−54] Finally, an alternative route consists in refining existing FFs by separately fitting those parameters that most influence the peculiar behavior of the molecule under study.

As a matter of fact, many studies were devoted to the development of reliable parameters consistent with the CHARMM,[55] UFF,[56] MM+,[57] and AMBER[31] FFs for nitroxide systems.[14,58−60] In particular, Houriez et al.[61] extended the CHARMM FF for a series of oxidanyl radicals, describing the nitrogen out-of-plane motion by a new functional form introduced in the original FF with different parameters for each nitroxide considered. In most recent research,[62,63] these authors dealt with DMPO derived spin adducts, specifically DMPO-OH and DMPO-OOH in water, concluding that in both cases there is no unique structure in aqueous solution responsible for the spectro-magnetic properties. Rather, an equilibrium between two major conformation sites has to be considered, and therefore the experimental hyperfine coupling constants can be interpreted as averages of those corresponding to different conformers of nitroxide five-member ring. In a parallel effort, our group has recently extended[22,23,27] the popular AMBER ff99SB FF[64,65] to both aliphatic and aromatic nitroxides obtaining remarkable results adding a minimal set of new parameters without any *ad hoc* potential term but explicitly including oxygen lone pairs.

From a different perspective, the effects of the vibrational averaging on the spectroscopic parameters can be taken into account by a time-independent approach using second-order vibrational perturbation theory (VPT2) for going beyond the harmonic approximation.[66,67] Both time-dependent and time-independent strategies have been extensively exploited in the last years for the prediction of molecular properties, such as chemical reactivity and spectroscopy.[66−74] In the framework of the Born−Oppenheimer approximation, once a reliable and correlation-consistent description of the PES is obtained, the method of choice for computing molecular vibrations is based on the solution of the Schrödinger equation. Semirigid molecules are usually well described by simple harmonic terms, possibly supplemented also by anharmonic terms issuing from an accurate yet feasible second-order perturbation scheme.[75] Spectroscopic observables are then computed through vibrational averaging with respect to molecular normal mode displacements, with temperature tuning the vibrational state population of each mode.[66]

The aim of the present work is to explore the application of both time-dependent and time-independent computational strategies to characterize vibrational averaging and environmental effects on the EPR parameters of the DMPO-H radical adduct (R = H in Figure 1), in benzene and water solutions. The present contribution goes beyond the mere reproduction of experimental results, by analyzing at the same time the roles that molecular dynamics and solvent play in tuning the magnetic properties. It is also worth noting that DMPO represents a very interesting system by itself because of its widespread experimental use as a spin trap, so that the hyperfine coupling constants of a large number of derived nitroxides are well-known under different experimental conditions. In particular, the DMPO-H radical is the simplest of these derived adducts, therefore representing a good test case for the validation of the proposed computational methodology aiming to treat more challenging nitroxide based radicals in complex environments.

2. COMPUTATIONAL METHODOLOGY

2.1. FF Parametrization. In order to employ the time-dependent strategy described in the Introduction, the AMBER FF was adopted, which relies on the simple potential energy function presented in eq 1:[50]

$$E_{\text{total}} = \sum_{\text{bonds}} k_r(r - r_0)^2 + \sum_{\text{angles}} k_\theta(\theta - \theta_0)^2 + \sum_{\text{dihedrals}} \frac{V_n}{2}[1 + \cos(n\varphi - \gamma)] + \sum_{i<j} \left\{ \frac{A_{ij}}{R_{ij}^{12}} - \frac{B_{ij}}{R_{ij}^{6}} + \frac{q_i q_j}{R_{ij}} \right\} \quad (1)$$

The first three summations run over bonds, angles, and torsions and represent the so-called valence terms. In the last term, the nonbonded interactions are computed through the sum of a Lennard-Jones potential and a standard Coulomb term. It may be worth noticing that the latter summation runs over atom pairs, excluding those separated by less than three bonds (1−2 and 1−3 interactions).

The partial atomic charges entering the Coulomb term were calculated with the restrained electrostatic potential (RESP) procedure,[76] by fitting an electrostatic potential grid computed for the nitroxide molecule at the HF/6-31G(d) level of theory.

The AMBER ff99SB parameter set has been recently extended[22,23,27] to reliably represent a large set of aminoxyl radicals, based on either aliphatic or aromatic rings. Unfortunately, none of the radicals of the training set employed therein present the peculiar feature of the DMPO-H molecule, i.e. hydrogen atoms in β position with respect to the NO-moiety. Considering the importance that these atoms may have in the determination of the hyperfine coupling constants, in this work AMBER ff99SB FF was further extended with a reliable parameter set for describing DMPO-H molecule, whose atom types are reported in Figure 2. In particular, new atom types representing the β-carbon (CL) and the two β-hydrogen atoms bonded to it (HM) have been added for an accurate reproduction of the molecular structure. Conversely, the NO-moiety has been described using specifically tailored parameters for the interaction involving NN, ON, and HN atom types in nitroxides.[22,23,27] The rest of the parameters are those of the original AMBER ff99SB FF. As in previous works on nitroxides,[22,23,27] in order to correctly represent the interaction between the NO-moiety and protic solvent molecules, explicit lone pairs (LP) have been introduced in the FF. Specifically, two lone pairs have been positioned at 0.45 Å from the oxygen atom, and with a N−O···LP angle of 120°, as is usual in the AMBER literature.[77] The minimal set of parameters involving the new sites introduced has been optimized for reproducing QM structural parameters and relative energies of the minimum energy conformation *in vacuo*, through a trial and error procedure.

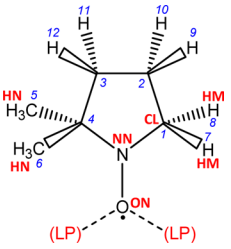

Figure 2. Structure and atom types in the AMBER ff99SB FF for the DMPO-H molecule. The atom types of nonlabeled carbon and hydrogen atoms are CT and HC, respectively.

All MM geometry optimizations were performed with the Gromacs4.5 engine,[78] exploiting the conjugate gradient minimization option.

2.2. QM Computational Details. The PBE0/N07D level of theory was employed for both geometry optimization and calculation of magnetic properties of DMPO-H nitroxide, with and without vibrational averaging at 298 K.

Several studies have shown that for semirigid molecules zero point vibrational (ZPV) contributions to different properties can be calculated in an accurate yet efficient way by employing second-order perturbation theory.[75,79,80] Briefly summarized, a property P is Taylor expanded around the equilibrium value in the normal coordinates describing the vibrational motion of the nuclei:

$$P = P_{\text{eq}} + \sum_i \left(\frac{\partial P}{\partial Q_i}\langle Q_i \rangle + \frac{\partial^2 P}{\partial Q_i^2}\langle Q_i^2 \rangle \right) \quad (2)$$

Using normal coordinates, Q_iQ_j terms vanish in the quadratic term whenever $i \neq j$ leading to simple functions of quadratic force constants, while the linear term contains the cubic force constants. The derivatives in eq 2 are found numerically using a central finite difference scheme. Consequently, the strategy here is to calculate the pure electronic contribution (at the equilibrium geometry) and then the vibrational contribution by eq 2. Note that the scheme is sufficiently general to work with most kinds of molecular properties.[75,79,81,82]

QM calculations were performed *in vacuo* and in two solvents, namely benzene and water. Bulk solvent effects were taken into account using the very effective polarizable continuum model (PCM).[37,83] In the case of water solution, the presence of explicit water molecules was also explored through the PCM/cluster approach, i.e. by handling explicitly at QM level the nearest solvent neighbors.

The PBE0/6-311+G(2df,2pd) level of theory[84,85] was employed to compute relative energies of DMPO-H nitroxide as a function of the out-of-plane dihedral.

The Gaussian09 suite of programs[86] has been used for all the QM calculations.

dx.doi.org/10.1021/ct4003256 | J. Chem. Theory Comput. 2013, 9, 3626−3636

2.3. MD Computational Details. In order to take into proper account both vibrational averaging effects and a reliable solvent distribution, classical MD simulations, employing the aforementioned FF refined for DMPO-H radical, have been performed *in vacuo* as well as in aqueous solution. MD runs *in vacuo* were performed in the canonical ensemble, whereas NPT ensemble was employed with water. Temperature (and pressure in NPT) was kept constant with the use of the weak coupling scheme of Berendsen et al.[87] Since no constraints were imposed on bond lengths of DMPO-H solute, a 0.2 fs time step was employed. Short-range interactions were truncated at R_c = 14 Å, employing standard corrections for energy and virial. Conversely, charge−charge long-range forces were treated with the particle mesh Ewald method[88,89] using convergence parameter α of $5.36/2R_c$ and a fourth-order spline interpolation.

For simulations in explicit water, periodic boundary conditions were applied and DMPO-H nitroxide was solvated into a cubic box containing 870 water molecules, described through the TIP3P model.[90] All runs were performed with the Gromacs4.5 code.[78]

2.4. Conformational Sampling. For both *in vacuo* and solvated simulation runs, magnetic parameters were computed on frames sampled from the last 2 ns of MD trajectories at regular time intervals of 10 ps. Isotropic hyperfine coupling constants were computed on snapshots extracted from MD trajectories following four different sampling schemes:

i. Frames containing only the solute nitroxide, extracted from the trajectory *in vacuo* ($MD_{intra/vacuum}$).

ii. Frames containing only the solute nitroxide, extracted from the trajectory in solvent by dropping all water molecules ($MD_{intra/solv}$).

iii. Frames containing the solute plus the two water molecules nearest to the oxygen atom, extracted from the trajectory in solvent ($MD_{cluster+2w}$).

iv. Frames containing the three molecules as in iii. plus the two water molecules that are nearest to each of the β-hydrogen atoms (totally six solvent molecules), extracted from the trajectory in solvent ($MD_{cluster+6w}$).

The reasons for the choice of the number of explicit water molecules to be included in the frame are clarified in the Results and Discussion section.

2.5. Hyperfine Splitting Calculation. An accurate calculation of isotropic hyperfine coupling constants should include both vibrational and solvent effects.

As the computation of the former is concerned, a fully consistent QM approach appears more rigorous and robust. The time-independent approach, described in the Introduction, offers this possibility. Hence, a first estimate of the hyperfine couplings can be obtained by anharmonic vibrationally averaging the DFT calculation performed *in vacuo*.

Indeed, the so-obtained value (labeled $a_{QM_{v.a.}}$ throughout the text) has to be corrected with the corresponding solvation term ($\Delta a_{solvent}$). This effect can in turn be evaluated as the sum of two components, direct ($\Delta a_{direct,solvent}$) and indirect ($\Delta a_{indirect,solvent}$). The former is the solvent effect itself on the computed couplings, while the latter accounts for the solute conformational changes, induced by the presence of the solvent, that also contributes to the final value. In the present work, the direct component can be estimated as

$$\Delta a_{direct,solvent} = a_{MDcluster+6w} - a_{MDintra/solv} \quad (3)$$

where $a_{MDcluster+6w}$ is the constant obtained averaging over frames containing both solute and (six, *vide infra*) explicit solvent molecules, whereas $a_{MDintra/solv}$ is computed from the snapshots with DMPO-H molecule alone ($MD_{intra/solv}$ distribution, see previous section). Conversely, the indirect component can be calculated as the difference between $a_{MDintra/solv}$ and the value obtained by averaging over frames extracted from an *in vacuo* MD, $a_{MDintra/vacuum}$, i.e.

$$\Delta a_{indirect,solvent} = a_{MDintra/solv} - a_{MDintra/vacuum} \quad (4)$$

In summary, the overall solvent effects on the hyperfine constant can be computed by combining eqs 3 and 4, i.e.

$$\Delta a_{solvent} = \Delta a_{direct,solvent} + \Delta a_{indirect,solvent} = a_{MDcluster+6w} - a_{MDintra/vacuum} \quad (5)$$

An accurate determination of the coupling constant can be achieved by exploiting a combination of the accuracy of a QM time-independent methodology, to account for vibrational averaging effects, with the capability of the time dependent statistical approach to include explicit solvent. With this aim, the best estimate of the isotropic hyperfine coupling constant, a_{final}, can be obtained as

$$a_{final} = a_{QM_{v.a.}} + \Delta a_{solvent} \quad (6)$$

3. RESULTS AND DISCUSSION

3.1. Extension of the AMBER Force Field. The computed partial atomic charges of DMPO-H radical adduct entering the Coulomb term of AMBER functional (eq 1) are listed in Table 1.

Table 1. RESP Partial Atomic Charges Computed on the DMPO-H Molecule at the HF/6-31G(d) Level of Theory

atom	partial atomic charge
C_1	0.057
$C_{2,3}$	−0.055
C_4	0.287
$C_{5,6}$	−0.106
$H_{7,8}$	0.075
$H_{9,10,11,12}$	0.005
N	0.080
O	−0.184
(LP)	−0.110

AMBER ff99SB FF parameters (extended to nitroxides for the HN, NN, and ON atom types[27]) were adopted as a starting guess for eq 1. As the parameters involving the new atom types CL and HM (representing the β-carbon and the two β-hydrogen atoms bonded to it, respectively) are concerned, the stretching and bending equilibrium values (*i.e.* r_0 and θ_0) were assigned from the QM equilibrium geometry, whereas all force constants and van der Waals parameters were initially transferred from the AMBER FF (setting CL = CT and HM = HC). Then, through a trial-and-error procedure, the latter parameters were refined to better represent the structure and relative energies of the QM minimum energy conformation. The parameters obtained, reported in Tables 2, 3, and 4, were then tested for reproducing the QM structure and the relative energies.

dx.doi.org/10.1021/ct4003256 | J. Chem. Theory Comput. 2013, 9, 3626−3636

Table 2. Bond Stretching and Bond Angle Parameters Involving the New Atom Types Reported in Figure 2

bond stretching	k_r/kcal mol^{-1} Å^{-2}	r_0/Å
CL−HM	358.5	1.100
CL−CT	310.7	1.515
CL−NN	370.5	1.460
angle bendings	k_θ/kcal mol^{-1} rad^{-2}	θ_0/deg
CT−CT−CL	40.0	109.5
CL−CT−HC	50.0	109.5
CT−CL−HM	50.0	109.5
CT−CL−NN	60.1	107.5
CT−NN−CL	52.6	120.8
CL−NN−ON	81.6	117.5
CL−CT−HN	50.0	109.5
HM−CL−HM	53.8	108.0
NN−CL−HM	65.7	109.2

Table 3. Dihedral and Improper Torsional Parameters Involving the New Atom Types Reported in Figure 2

regular torsion	$V_n/2$ (kcal mol^{-1})	φ/deg	n
CL−CT−CT−CT	0.200	0.0	1
	0.250	180.0	2
	0.180	180.0	3
CT−CT−CL−NN	0.143	0.0	3
CT−CT−CT−HN	0.160	0.0	3
CT−CT−CL−HM	0.160	0.0	3
NN−CL−CT−HC	0.100	0.0	3
HC−CT−CT−HC	0.150	0.0	3
HM−CL−CT−HC	0.150	0.0	3
CL−NN−CT−CT	0.034	0.0	3
CT−NN−CL−CT	0.034	0.0	3
CT−NN−CL−HM	0.034	0.0	3
ON−NN−CL−CT	0.034	0.0	3
ON−NN−CL−HM	0.034	0.0	3
CT−NN−ON−LP	0.000	0.0	3
CL−NN−ON−LP	0.000	0.0	3
improper torsions	$V_n/2$ (kcal mol^{-1})	φ/deg	n
CT−CL−NN−ON	2.000	180.0	2

Table 4. van der Waals Parameters of the New Atom Types

nonbond interactions	R^{*a}/Å	ε^b / kcal mol^{-1}
CL	1.908	0.1094
HM	1.263	0.0157

$^a R^*_{ij} = R^*_i + R^*_j$. $^b \varepsilon_{ij} = (\varepsilon_i \varepsilon_j)^{1/2}$, $A_{ij} = \varepsilon_{ij}(R^*_{ij})^{12}$ and $B_{ij} = 2\varepsilon_{ij}(R^*_{ij})^6$.

The structural features (bond lengths, bond angles, and dihedral angles) calculated after geometry optimization at the MM level can be compared with their QM counterparts, at the PBE0/N07D level of theory, from data collected in Table 5. The remarkable agreement between both sets of data is apparent; differences in bond lengths and angles are smaller than 0.01 Å and 3.2°, respectively, whereas higher discrepancies are found in dihedral angles. However, given the simplicity of the functional form used, it is possible to consider that the fitting was done correctly. Nevertheless, since the nitrogen hyperfine coupling constant clearly depends on the N−O bond length and the out-of-plane angle (C_4−C_1−N−O), it is worth noting that both are quite close to QM data. Besides, the variation of the relative energies with the out-of-plane angle is also correctly reproduced by the new FF, as it is observed in Figure 3.

To further validate the accuracy of the refined FF, EPR parameters of DMPO-H radical were computed at the PBE0/N07D level of theory *in vacuo* on the MM optimized structure and compared to those calculated on the QM minimum. The isotropic hyperfine coupling constants computed on the MM geometry are 11.4 G for the nitrogen atom (a_N) and 18.5 G for the β-hydrogen atoms (a_H in average), reproducing very well the values of 11.5 and 17.9 G, respectively, obtained on the QM minimum.

3.2. Solvent Effects on EPR Parameters. As mentioned above, nitroxides are usually employed in different solvents. It is therefore crucial that EPR parameters are well reproduced not only *in vacuo* but also when the radicals are embedded in different solvents. However, the values of the magnetic parameters of DMPO-H calculated *in vacuo* are far from their experimental counterparts in benzene and water (14.43 and 16.6 G for a_N and 18.89 and 22.5 G for a_H, respectively).[91,92] To further characterize the effect of the solvent on magnetic parameters, geometry optimization at QM level was performed in benzene and water as well. In the case of benzene, only the conventional PCM model was employed to consider bulk solvent effect, whereas both the explicit and implicit approaches were used for aqueous solution to account for the polar interaction. Indeed, a first calculation was performed by handling bulk solvent effects with conventional PCM. However, spectroscopic observations unequivocally show that two water molecules are strongly and specifically bound to the oxygen in this kind of systems.[93] Therefore, reoptimization of the DMPO-H adduct with two explicit water molecules representing the closest solvent shell was performed.

The position of the water molecules in the minimum-energy structure, represented in Figure 4, is similar to that previously obtained in other nitroxides,[27] with analogous geometrical features of the solvated region. The directionality of the two water molecules involved in hydrogen bonding is well reproduced. Both of them lie in the plane defined by N−O−LP approximately along the directions of the two lone pairs. On this geometry, a cluster-PCM approach, consisting of DMPO-H plus two explicit water molecules (PCM+2w) was adopted for a better description of the microsolvation. As shown in Table 5, the most relevant features of the DMPO-H molecular geometry are almost independent of solvent effects, whatever it is the selected method to include the solvation (maximum differences of 0.01 Å in distances and 3.1° in angles). This is a remarkable result, since it allows us to evaluate dynamical effects in the gas phase and add a posteriori static solvent shifts to the averaged results, as detailed in eqs 3−6. As regards the geometries obtained by the three methods considered to take into account water solvent effect, it is important to remark that the differences in geometrical parameters among them are negligible.

EPR parameters of DMPO-H radical adduct were then computed on the MM (MM_{PCM}) and all the QM equilibrium conformations with implicit and/or explicit solvation, *i.e. (i)* PCM method (QM_{PCM}), *(ii)* explicit inclusion of the two water molecules in the QM calculation (QM_{2w}), and *(iii)* a combination of implicit and explicit water solvent (QM_{PCM+2w}). The resulting isotropic coupling constants are listed in Table 6.

The effect of PCM solvation on the hyperfine constants is clear: the value increases by ∼0.8 G when passing from vacuum to benzene and approximately double in the case of water

dx.doi.org/10.1021/ct4003256 | J. Chem. Theory Comput. 2013, 9, 3626−3636

Table 5. Geometrical Parameters of DMPO-H Nitroxide Structure Optimized at QM (PBE0/N07D), MM Levels of Theory, and Averaged over MD Runs (Distances in Å and Angles in degree)

	vacuum			benzene	water			
	QM	MM	⟨MD⟩	QM_{PCM}	QM_{PCM}	QM_{2w}	QM_{PCM+2w}	⟨MD⟩
N−O	1.26	1.27	1.26 ± 0.02	1.26	1.26	1.27	1.27	1.27 ± 0.03
$N-C_1$	1.46	1.45	1.45 ± 0.02	1.46	1.46	1.46	1.46	1.45 ± 0.03
C_1-C_2	1.52	1.52	1.52 ± 0.02	1.52	1.52	1.52	1.52	1.52 ± 0.03
C_2-C_3	1.53	1.54	1.54 ± 0.02	1.53	1.53	1.53	1.53	1.54 ± 0.03
C_3-C_4	1.54	1.55	1.55 ± 0.02	1.54	1.54	1.54	1.54	1.55 ± 0.03
$N-C_4$	1.48	1.49	1.49 ± 0.02	1.48	1.48	1.48	1.48	1.49 ± 0.03
C_1-H_7	1.10	1.10	1.10 ± 0.02	1.09	1.09	1.09	1.09	1.10 ± 0.03
$O-N-C_1$	122.9	121.2	120.3 ± 1.8	122.8	122.7	122.2	122.4	119.8 ± 2.7
$O-N-C_4$	122.7	123.4	123.1 ± 1.7	122.8	122.9	123.1	123.0	122.6 ± 2.8
$N-C_1-H_7$	109.2	110.3	110.6 ± 2.2	109.2	109.3	109.4	109.3	110.4 ± 3.6
$N-C_1-C_2$	103.2	103.6	104.4 ± 1.3	103.2	103.2	102.8	102.8	103.2 ± 2.9
$C_1-C_2-C_3$	103.6	106.8	107.0 ± 1.7	103.5	103.5	103.4	103.4	106.9 ± 3.0
$N-C_4-C_3$	101.2	102.4	103.1 ± 1.3	101.1	101.1	100.6	100.8	101.6 ± 2.6
$H_7-C_1-H_8$	108.0	109.9	109.3 ± 2.0	108.1	108.3	107.6	108.5	109.6 ± 3.9
$H_{10}-C_2-H_9$	107.6	109.7	109.6 ± 2.7	107.7	107.8	107.7	107.9	109.3 ± 4.6
$H_{11}-C_3-H_{12}$	107.7	108.7	108.1 ± 2.8	107.8	107.9	107.8	107.9	107.7 ± 4.6
$C_5-C_4-C_6$	110.6	110.8	110.5 ± 2.4	110.6	110.7	110.9	111.0	110.8 ± 3.6
$N-C_1-C_2-C_3$	−28.5	−21.6	−3.6 ± 17.6[a]	−28.6	−28.8	−29.4	−29.5	−1.6 ± 20.1[a]
$C_1-C_2-C_3-C_4$	36.4	25.8	3.6 ± 18.4[a]	36.5	36.6	37.2	37.0	−1.4 ± 22.7[a]
$O-N-C_1-H_7$	−43.5	−51.6	−58.9 ± 14.6	−44.0	−44.8	−46.1	−45.2	−59.9 ± 19.4
C_4-C_1-N-O	−176.6	179.0	3.7 ± 167.9[a]	−177.4	−178.3	−179.3	−179.7	−1.7 ± 167.3[a]

[a]Values were averaged over two separate distribution peaks (see details in the text).

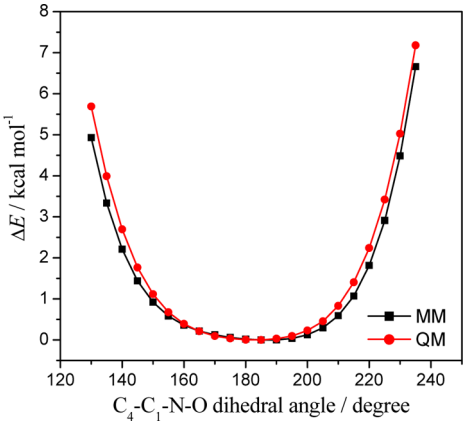

Figure 3. Comparison between QM (PBE0/6-311+G(2df,2pd)//PBE0/N07D) and MM relative energies of DMPO-H nitroxide as a function of the C_4-C_1-N-O out-of-plane dihedral.

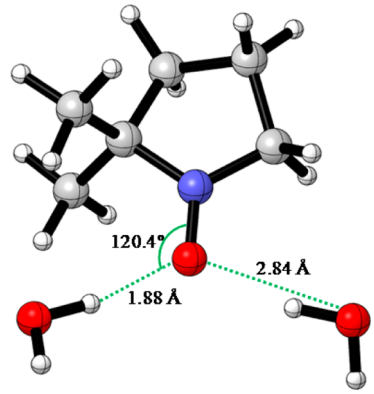

Figure 4. Optimized structure (PBE0/N07D) of DMPO-H adduct with two water molecules.

solution treated at the PCM level; the same trend is observed for both QM and MM optimized structures. Inclusion of explicit solvation raises the values by a significant amount (a_N and a_H are, respectively, 1.5 and 0.9 G higher in QM_{PCM+2w} than in QM_{PCM}), which allows us to point out that the incorporation of coordinating water molecules is mandatory for a proper description of the magnetic parameters of this system. However, comparison of all these results with their experimental counterparts shows that the data are still underestimated by an important quantity (2.3 G for a_N and 1.3 G for a_H). It seems that, apart from environmental effects, a proper account of dynamical effect (i.e., molecular vibrations) is also required.

3.3. Dynamical Effects on EPR Parameters. On these grounds, classical molecular dynamics simulations were performed, both *in vacuo* and water solvent. The average values of DMPO-H internal coordinates computed over both trajectories are reported in Table 5. These values are mostly in good agreement with QM optimized geometry, oscillating

Table 6. Isotropic Hyperfine Coupling Constants (in Gauss) of DMPO-H Nitroxide, Computed at the PBE0/N07D Level of Theory, on the QM and MM Optimized Structures in Benzene and Water Solvents

solvent	solvation model	a_N	a_H
benzene	QM_{PCM}	12.2	18.7
	MM_{PCM}	12.1	19.4
	experimental[91]	14.43	18.89
water	QM_{PCM}	12.9	19.4
	MM_{PCM}	12.8	20.3
	QM_{2w}	13.5	20.4
	QM_{PCM+2w}	14.3	21.2
	experimental[92]	16.6	22.5

dx.doi.org/10.1021/ct4003256 | J. Chem. Theory Comput. 2013, 9, 3626−3636

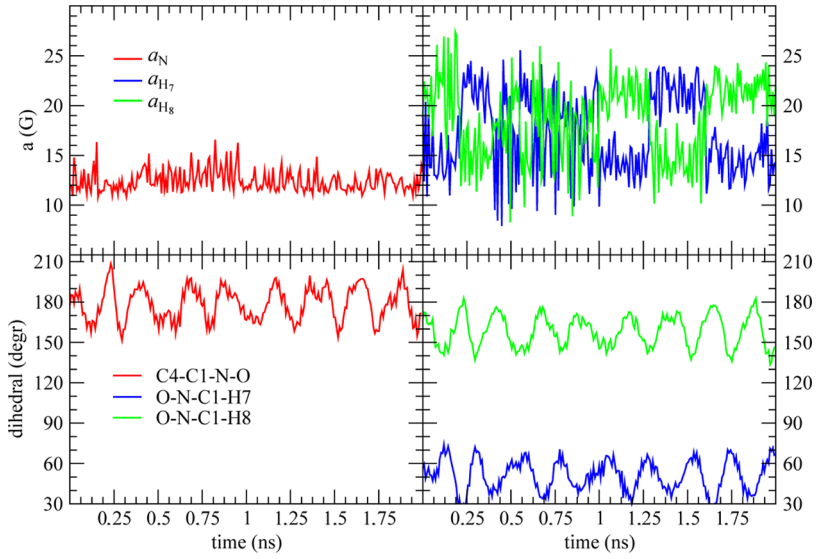

Figure 5. Top panels: hyperfine coupling constants computed on MD trajectory as a function of simulation time. Bottom panels: dihedral angle values computed over the same trajectory. All calculations refer to MD *in vacuo*.

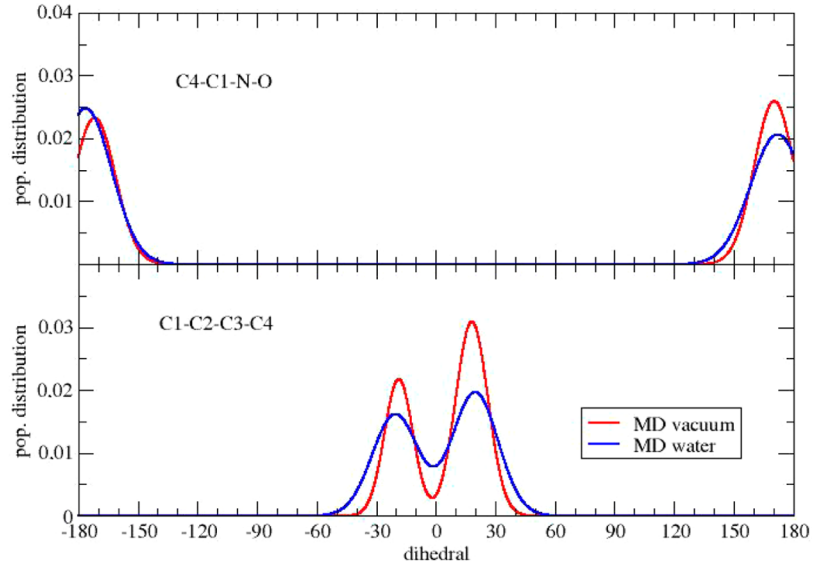

Figure 6. Distribution of out-of-plane (C_4-C_1-N-O) and backbone ($C_1-C_2-C_3-C_4$) dihedral angles over MD trajectories *in vacuo* (red lines) and water solvent (blue lines).

around their mean value with relatively small amplitude, except for the torsions around the dihedral angles. These oscillations are expected to be important in accounting for hyperfine constants, as they involve atoms relevant to the coupling. In the bottom panels of Figure 5, the values of some selected dihedral angles, computed for all frames of the MD trajectory *in vacuo*, are reported as a function of time. Its dynamics clearly reflects in a broad distribution of the hyperfine constants, especially remarkable in case of a_H, computed over the same trajectory and reported in the top panels of the same figure. Since this analysis was performed on the run without the solvent molecules, the important role played by intramolecular dynamics in determining the coupling constants is confirmed.

For a preliminary evaluation of the solvent effect over the internal dynamics, the population distribution of all dihedral angles was computed over both MD trajectories (*in vacuo* and water) and reported in Figure 6 for dihedral angles driving the out-of-plane vibration of the oxygen atom (C_4-C_1-N-O) and the backbone conformational motion ($C_1-C_2-C_3-C_4$). Similar results were obtained for other torsions. Figure 6 clearly shows that there are two populated distributions; therefore, the values of the dihedral angles listed in Table 5 are the averages over the two corresponding peaks. Both most populated peaks (~180° and ±25°, for C_4-C_1-N-O and $C_1-C_2-C_3-C_4$, respectively) are in good agreement with QM minimum structure, but the sampling also includes other geometries, effectively populated in the employed thermodynamic conditions. As far as the solvent effect is concerned, the collisions with the neighboring water molecules induce the enlargement of the bandwidth, a result that is more pronounced on the backbone dihedral angle. It can be speculated that the latter difference is due to the stronger interaction stemming from hydrogen bonds between the water molecules and the oxygen atom, which is in turn the most directly involved in the out-of-plane vibration.

dx.doi.org/10.1021/ct4003256 | J. Chem. Theory Comput. 2013, 9, 3626−3636

With the 2-fold aim to verify the above hypothesis and the choice of the number of water molecules to be explicitly included in the PCM/cluster model, atom−atom pair correlation function was computed over MD trajectories and the average number of hydrogen bonds was also estimated through geometrical criteria.[78] This average was 1.7, in agreement with experimental evidence on aqueous nitroxides which pointed out that water forms two hydrogen bonds with the NO-moiety.[93] However, as shown in Figure 7, in which the

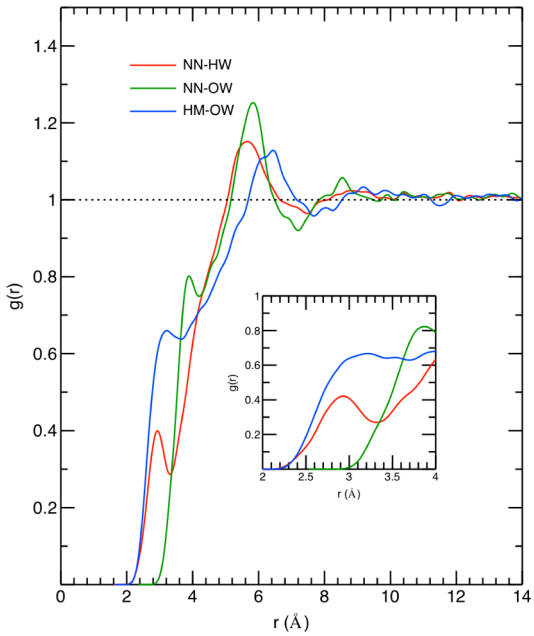

Figure 7. Atom-atom pair correlation functions computed over the MD trajectory in water solvent. Water hydrogen (HW) and oxygen (OW) atoms have been correlated with the N atom (NN) of the DMPO-H solute (red and green lines, respectively). The blue line indicates the pair correlation function between OW and the β-hydrogen (HM) of the radical.

pair correlation functions between selected atom pairs have been reported, water oxygen atoms are also found very near the β-hydrogens. This result suggests that the presence of more than two water molecules should be taken into account. For these reasons, MD simulation was also performed on a cluster with six explicit water molecules, $MD_{cluster+6w}$, selected as described in the Computational Methodology section.

The hyperfine coupling constants were computed on the frames extracted from the *in vacuo* MD ($MD_{intra/vacuum}$) and on the other three sets of frames extracted from the MD in water, according to the $MD_{intra/solv}$, $MD_{cluster+2w}$, and $MD_{cluster+6w}$ schemes. All results are summarized in Table 7.

Averaging along MD simulation leads to an overall vibrational correction of the nitrogen hyperfine constant of 0.9 G in benzene solvent, and surprisingly has no effect on a_H. In the case of water, as found in the QM calculations, the values obtained with the four MD simulations analyzed also prove the necessity of inclusion of the six explicit water molecules, since both a_N and a_H improve considerably with the explicit solvation. Averaging of classical MD gives rise to a_N and a_H values of 15.3 and 20.3 G, respectively, which are closer to the corresponding experimental data.

A time-independent approach was also applied to DMPO-H nitroxide to quantify the effects of molecular dynamics on the

Table 7. Isotropic Hyperfine Coupling Constants (in Gauss) of DMPO-H Nitroxide Computed at the PBE0/N07D Level of Theory and Averaged over Frames Extracted from MD Trajectories *in Vacuo* and Water Solvent

solvent	solvation model	a_N	a_H
vacuum	$QM//MD_{intra/vacuum}$	12.4	17.9
benzene	$QM_{PCM}//MD_{intra/vacuum}$	13.1	18.7
	experimental[91]	14.43	18.89
water	$QM_{PCM}//MD_{intra/vacuum}$	12.4	17.8
	$QM_{PCM}//MD_{intra/solv}$	12.7	16.8
	$QM_{PCM}//MD_{cluster+2w}$	15.0	19.9
	$QM_{PCM}//MD_{cluster+6w}$	15.3	20.3
	experimental[92]	16.6	22.5

spectroscopic parameters, which are computed through QM vibrational averaging with respect to the molecular normal modes, with temperature tuning the population of each mode. The vibrationally averaged coupling constants calculated *in vacuo* and with PCM solvation are collected in Table 8. The

Table 8. Isotropic Hyperfine Coupling Constants (in Gauss) of DMPO-H Nitroxide Computed at the PBE0/N07D Level of Theory Including Quantum Vibrational Averaging at 298 K, *in Vacuo*, and Benzene and Water Solvents

solvent	a_N	a_H
vacuum	13.2	16.8
PCM-benzene	13.7	15.8
PCM-water	14.0	16.9

vibrational effect on a_N implies an increase of 1.5 and 1.1 G for calculations in benzene and water (PCM), respectively, and a decrease of 2.9 and 2.5 G on a_H; as expected, the effect is less intense as the interaction of the molecule with the surroundings becomes stronger. In the case of aqueous solution, more accurate values could be obtained by performing the calculation with the inclusion of explicit water molecules. Unfortunately, some of the cluster normal modes are linear combinations of intermolecular distances between the nitroxide and the water molecules, described by large amplitude motions, which cannot be accurately handled within a harmonic treatment. Nevertheless, as previously indicated, it is also possible to resort to a combined approach that consists of computing separately vibrational (using time-independent route *in vacuo*) and solvent effects (as difference between MD with and without solvation).

As Table 9 summarizes, in the case of aqueous solution, direct and indirect components are, respectively, 2.6 and 0.3 G for a_N and 3.5 and −1.0 G for a_H. Thus, the total water correction terms amount to 2.9 and 2.5 G, respectively, whereas the solvent shift is of only 0.7−0.8 G for benzene solution (only the whole solvent effect can be evaluated for benzene as a solvent, although the indirect term is expected to be negligible). Final a_N values so estimated are 13.9 and 16.1 G for benzene and water solutions, respectively, which are in remarkable agreement with their experimental counterparts. However, the discrepancy is greater in the case of a_H (1.3 and 3.2 G for benzene and water, respectively). This can be due to the much higher standard deviation of a_H values compared to those of a_N (for instance, in $MD_{cluster+6w}$, the value of a_N is 15.3 ± 1.6 G whereas a_H = 20.3 ± 6.0 G). This latter value is in accordance with the high sensitivity of a_H to distortions of molecular

dx.doi.org/10.1021/ct4003256 | J. Chem. Theory Comput. 2013, 9, 3626−3636

Table 9. Dynamics and Solvent Contributions to the Isotropic Hyperfine Coupling Constant (In Gauss) of DMPO-H Nitroxide

	$a_{QM_{v.a.}}$	$\Delta a_{direct,solvent}$	$\Delta a_{indirect,solvent}$	$\Delta a_{solvent}$	a_{final}	exp[91,92]
Nitrogen						
benzene	13.2	---	---	0.7	13.9	14.43
water		2.6	0.3	2.9	16.1	16.6
Hydrogen						
benzene	16.8	---	---	0.8	17.6	18.89
water		3.5	−1.0	2.5	19.3	22.5

geometry, leading to a broader distribution of both a_H compared to that of a_N, as shown in Figure 5.

4. CONCLUSIONS

In the present paper, a computational strategy, combining time-dependent and time-independent approaches, has been proposed and validated for accurately modeling the effects of dynamics and of solvent on the magnetic properties of the DMPO-H nitroxide.

Our previous nitroxide force field (based on the AMBER ff99SB background) was further extended to β-hydrogen atoms. The isotropic hyperfine coupling constants computed at the PBE0/N07D level of theory on the geometries optimized at the MM level provide results in excellent agreement with those calculated on the QM optimized structures.

The new force field has been employed in a series of classical molecular dynamics simulations to compute EPR parameters in different solvents. The bulk solvent effects have been taken into account by the PCM, and, when needed, explicit first-solvent shell molecules have been also included. The results clearly point out the necessity of explicitly integrating some of the interactions to correctly reproduce experimental data.

The effects of the vibrational averaging on the spectroscopic parameters have been taken into account also by a time-independent calculation *in vacuo*. The issuing hyperfine constants further corrected with the solvation term estimated by the time-dependent approach are in remarkable agreement with the corresponding experimental data, thus confirming the effectiveness of the proposed computational strategy for the accurate modeling of dynamic and solvent effects on the magnetic properties of this kind of nitroxides.

■ ASSOCIATED CONTENT

Supporting Information

Vibrational harmonic frequencies of DMPO-H nitroxide *in vacuo* computed at PBE0/N07D level of theory; the intramolecular parameters for extending the force-field to DMPO-H nitroxide. This material is available free of charge via the Internet at http://pubs.acs.org.

■ AUTHOR INFORMATION

Corresponding Author

*E-mail: laura.hermosilla@uam.es (L.H.), giacomo.prampolini@pi.ipcf.cnr.it (G.P.).

Notes

The authors declare no competing financial interest.

■ ACKNOWLEDGMENTS

This work was supported by European Union (ERC-2012-AdG-320951-DREAMS grant) and by the Spain MICINN (CTQ2010-1923 and MAT2011-29174-C02-02). The high performance computer facilities of the DREAMS center (http://dreamshpc.sns.it) are acknowledged for providing computer resources. The support of COST-CMTS Action CM1002 "COnvergent Distributed Environment for Computational Spectroscopy (CODECS)" is also acknowledged.

■ REFERENCES

(1) Kocherginsky, N.; Swartz, H. M. *Nitroxide Spin Labels: Reactions in Biology and Chemistry*; CRC Press: New York, 1995.
(2) Buchaklian, A. H.; Klug, C. S. *Biochemistry* **2005**, *44*, 5503−5509.
(3) Rassat, A. *Pure Appl. Chem.* **1990**, *62*, 223−227.
(4) Buettner, G. R. *Free Radical Biol. Med.* **1987**, *3*, 259−303.
(5) Tedeschi, A. M.; D'Errico, G.; Busi, E.; Basosi, R.; Barone, V. *Phys. Chem. Chem. Phys.* **2002**, *4*, 2180−2188.
(6) Likhtenshtein, G.; Yamauchi, J.; Nakatsuji, S.; Smirnov, A. I.; Tamura, R. *Nitroxides: Applications in Chemistry, Biomedicine, and Materials Science*; John Wiley & Sons: Weinheim, 2008.
(7) *Spin labelling: Theory and Applications*; Berliner, L. J., Ed.; Academic Press: New York, 1976.
(8) Carlotto, S.; Cimino, P.; Zerbetto, M.; Franco, L.; Corvaja, C.; Crisma, M.; Formaggio, F.; Toniolo, C.; Polimeno, A.; Barone, V. *J. Am. Chem. Soc.* **2007**, *129*, 11248−11258.
(9) Improta, R.; Barone, V. *Chem. Rev.* **2004**, *104*, 1231−1253.
(10) Barone, V.; Polimeno, A. *Phys. Chem. Chem. Phys.* **2006**, *8*, 4609−4629.
(11) Ciofini, I.; Adamo, C.; Barone, V. *J. Chem. Phys.* **2004**, *121*, 6710−6718.
(12) Adamo, C.; Di Matteo, A.; Rey, P.; Barone, V. *J. Phys. Chem. A* **1999**, *103*, 3481−3488.
(13) Di Matteo, A.; Adamo, C.; Cossi, M.; Barone, V.; Rey, P. *Chem. Phys. Lett.* **1999**, *310*, 159−165.
(14) Barone, V.; Bencini, A.; Cossi, M.; Di Matteo, A.; Mattesini, M.; Totti, F. *J. Am. Chem. Soc.* **1998**, *120*, 7069−7078.
(15) Cirujeda, J.; Vidal-Gancedo, J.; Jurgens, O.; Mota, F.; Novoa, J. J.; Rovira, C.; Veciana, J. *J. Am. Chem. Soc.* **2000**, *122*, 11393−11405.
(16) Zheludev, A.; Barone, V.; Bonnet, M.; Delley, B.; Grand, A.; Ressouche, E.; Rey, P.; Subra, R.; Schweizer, J. *J. Am. Chem. Soc.* **1994**, *116*, 2019−2027.
(17) Zerbetto, M.; Polimeno, A.; Barone, V. *Comput. Phys. Commun.* **2009**, *180*, 2680−2697.
(18) Barone, V.; Cimino, P.; Pavone, M. EPR Spectra of Organic Free Radicals in Solution From an Integrated Computational Approach. In *Continuum Solvation Models in Chemical Physics*; Mennucci, B., Cammi, R., Eds.; John Wiley & Sons, Ltd.: Chichester, 2007; pp 145−166.
(19) Villamena, F. A.; Liu, Y.; Zweier, J. L. *J. Phys. Chem. A* **2008**, *112*, 12607−12615.
(20) Stipa, P. *Chem. Phys.* **2006**, *323*, 501−510.
(21) Beyer, M.; Fritscher, J.; Feresin, E.; Schiemann, O. *J. Org. Chem.* **2003**, *68*, 2209−2215.
(22) Cimino, P.; Pedone, A.; Stendardo, E.; Barone, V. *Phys. Chem. Chem. Phys.* **2010**, *12*, 3741−3746.
(23) Grubisic, S.; Brancato, G.; Pedone, A.; Barone, V. *Phys. Chem. Chem. Phys.* **2012**, *14*, 15308−15320.
(24) Rajca, A.; Vale, M.; Rajca, S. *J. Am. Chem. Soc.* **2008**, *130*, 9099−9105.
(25) Hermosilla, L.; Calle, P.; Garcia de la Vega, J. M.; Sieiro, C. *J. Phys. Chem. A* **2006**, *110*, 13600−13608.

(26) Hermosilla, L.; Garcia de la Vega, J. M.; Sieiro, C.; Calle, P. *J. Chem. Theory Comput.* **2011**, *7*, 169−179.
(27) Stendardo, E.; Pedone, A.; Cimino, P.; Menziani, M. C.; Crescenzi, O.; Barone, V. *Phys. Chem. Chem. Phys.* **2010**, *12*, 11697−11709.
(28) Barone, V.; Cimino, P.; Crescenzi, O.; Pavone, M. *J. Mol. Struct.: THEOCHEM* **2007**, *811*, 323−335.
(29) Barone, V.; Cimino, P.; Stendardo, E. *J. Chem. Theory Comput.* **2008**, *4*, 751−764.
(30) Barone, V.; Cimino, P. *Chem. Phys. Lett.* **2008**, *454*, 139−143.
(31) Barone, V.; Cimino, P. *J. Chem. Theory Comput.* **2009**, *5*, 192−199.
(32) Puzzarini, C.; Barone, V. *J. Chem. Theory Comput.* **2009**, *5*, 2378−2387.
(33) Puzzarini, C.; Biczysko, M.; Barone, V. *J. Chem. Theory Comput.* **2010**, *6*, 828−838.
(34) Barone, V.; Bloino, J.; Biczysko, M. *Phys. Chem. Chem. Phys.* **2010**, *12*, 1092−1101.
(35) Houriez, C.; Ferre, N.; Flament, J. P.; Masella, M.; Siri, D. *J. Phys. Chem. A* **2007**, *111*, 11673−11682.
(36) Miertus, S.; Scrocco, E.; Tomasi, J. *Chem. Phys.* **1981**, *55*, 117−129.
(37) Tomasi, J.; Mennucci, B.; Cammi, R. *Chem. Rev.* **2005**, *105*, 2999−3093.
(38) Adamo, C.; Cossi, M.; Rega, N.; Barone, V. New Computational Strategies for the Quantum Mechanical Study of Biological Systems in Condensed Phases. In *Theoretical Biochemistry: Processes and Properties of Biological Systems*; Eriksson, L. A., Ed.; Elsevier: New York, 2001; pp 467−538.
(39) Cossi, M.; Scalmani, G.; Rega, N.; Barone, V. *J. Chem. Phys.* **2002**, *117*, 43−54.
(40) Cossi, M.; Barone, V. *J. Chem. Phys.* **2001**, *115*, 4708−4717.
(41) Adamo, C.; Barone, V. *Chem. Phys. Lett.* **2000**, *330*, 152−160.
(42) Aquilante, F.; Barone, V.; Roos, B. O. *J. Chem. Phys.* **2003**, *119*, 12323−12334.
(43) Koch, A.; Thomas, S.; Kleinpeter, E. *J. Mol. Struct.: THEOCHEM* **1997**, *401*, 1−14.
(44) Saracino, G. A. A.; Tedeschi, A.; D'Errico, G.; Improta, R.; Franco, L.; Ruzzi, M.; Corvaia, C.; Barone, V. *J. Phys. Chem. A* **2002**, *106*, 10700−10706.
(45) Pavone, M.; Cimino, P.; Crescenzi, O.; Sillanpaeae, A.; Barone, V. *J. Phys. Chem. B* **2007**, *111*, 8928−8939.
(46) Car, R.; Parrinello, M. *Phys. Rev. Lett.* **1985**, *55*, 2471−2474.
(47) Pavone, M.; Benzi, C.; De Angelis, F.; Barone, V. *Chem. Phys. Lett.* **2004**, *395*, 120−126.
(48) Pavone, M.; Cimino, P.; De Angelis, F.; Barone, V. *J. Am. Chem. Soc.* **2006**, *128*, 4338−4347.
(49) Pavone, M.; Sillanpaa, A.; Cimino, P.; Crescenzi, O.; Barone, V. *J. Phys. Chem. B* **2006**, *110*, 16189−16192.
(50) Cornell, W. D.; Cieplak, P.; Bayly, C. I.; Gould, I. R.; Merz, K. M.; Ferguson, D. M.; Spellmeyer, D. C.; Fox, T.; Caldwell, J. W.; Kollman, P. A. *J. Am. Chem. Soc.* **1995**, *117*, 5179−5197.
(51) Halgren, T. A. *J. Comput. Chem.* **1996**, *17*, 490−519.
(52) Barone, V.; Cacelli, I.; De Mitri, N.; Licari, D.; Monti, S.; Prampolini, G. *Phys. Chem. Chem. Phys.* **2013**, *15*, 3736−3751.
(53) Cacelli, I.; Prampolini, G. *J. Chem. Theory Comput.* **2007**, *3*, 1803−1817.
(54) Ewig, C. S.; Berry, R.; Dinur, U.; Hill, J.-R.; Hwang, M.-J.; Li, H.; Liang, C.; Maple, J.; Peng, Z.; Stockfisch, T. P.; Thacher, T. S.; Yan, L.; Ni, X.; Hagler, A. T. *J. Comput. Chem.* **2001**, *22*, 1782−1800.
(55) MacKerell, A. D., Jr.; Brooks, B.; Brooks, C. L., III; Nilsson, L.; Roux, B.; Won, Y.; Karplus, M. The Energy Function and its Parameterization with an Overview of the Program. In *The Encyclopedia of Computational Chemistry*; Schleyer, P. v. R., Ed.; John Wiley & Sons: Chichester, 1998; pp 271−277.
(56) Rappe, A. K.; Casewit, C. J.; Colwell, K. S.; Goddard, W. A.; Skiff, W. M. *J. Am. Chem. Soc.* **1992**, *114*, 10024−10035.
(57) Holloway, M. K.; Wai, J. M.; Halgren, T. A.; Fitzgerald, P. M. D.; Vacca, J. P.; Dorsey, B. D.; Levin, R. B.; Thompson, W. J.; Chen, L. J.; Desolms, S. J.; Gaffin, N.; Ghosh, A. K.; Giuliani, E. A.; Graham, S. L.; Guare, J. P.; Hungate, R. W.; Lyle, T. A.; Sanders, W. M.; Tucker, T. J.; Wiggins, M.; Wiscount, C. M.; Woltersdorf, O. W.; Young, S. D.; Darke, P. L.; Zugay, J. A. *J. Med. Chem.* **1995**, *38*, 305−317.
(58) Improta, R.; di Matteo, A.; Barone, V. *Theor. Chem. Acc.* **2000**, *104*, 273−279.
(59) Houriez, C.; Ferre, N.; Masella, M.; Siri, D. *J. Chem. Phys.* **2008**, *128*, 244504.
(60) Sezer, D.; Freed, J. H.; Roux, B. *J. Phys. Chem. B* **2008**, *112*, 5755−5767.
(61) Houriez, C.; Ferre, N.; Siri, D.; Masella, M. *J. Phys. Chem. B* **2009**, *113*, 15047−15056.
(62) Houriez, C. l.; Ferré, N.; Siri, D.; Tordo, P.; Masella, M. *J. Phys. Chem. B* **2010**, *114*, 11793−11803.
(63) Houriez, C.; Ferré, N.; Siri, D.; Tordo, P.; Masella, M. *Theor. Chem. Acc.* **2012**, *131*, 1−5.
(64) Hornak, V.; Abel, R.; Okur, A.; Strockbine, B.; Roitberg, A.; Simmerling, C. *Proteins* **2006**, *65*, 712−725.
(65) Case, D. A.; Darden, T. A.; Cheatham, T. E.; Simmerling, C. L.; Wang, J.; Duke, R. E.; Luo, R.; Crowley, M.; Walker, R. C.; Zhang, W.; Merz, K. M.; Wang, B.; Hayik, S.; Roitberg, A.; Seabra, G.; Kolossvai, I.; Wong, K. F.; Paesani, F.; Vanicek, J.; Wu, X.; Brozell, S. R.; Steibrecher, T.; Gohlke, H.; Yang, L.; Tan, C.; Mongan, J.; Hornak, V.; Cui, G.; Mathews, D. H.; Seetin, M. G.; Sagui, C.; Babin, V.; Kollman, P. A. *AMBER 10*; University of California: San Francisco, 2008.
(66) Barone, V. *J. Chem. Phys.* **2005**, *122*, 014108.
(67) Pavone, M.; Biczysko, M.; Rega, N.; Barone, V. *J. Phys. Chem. B* **2010**, *114*, 11509−11514.
(68) Iyengar, S. S. *J. Chem. Phys.* **2005**, *123*, 084310.
(69) Iyengar, S. S.; Petersen, M. K.; Day, T. J. F.; Burnham, C. J.; Teige, V. E.; Voth, G. A. *J. Chem. Phys.* **2005**, *123*, 084309.
(70) Iyengar, S. S. *J. Chem. Phys.* **2007**, *126*, 216101.
(71) Li, X.; Teige, V. E.; Iyengar, S. S. *J. Phys. Chem. A* **2007**, *111*, 4815−4820.
(72) Li, X.; Moore, D. T.; Iyengar, S. S. *J. Chem. Phys.* **2008**, *128*, 184308.
(73) Barone, V.; Bloino, J.; Monti, S.; Pedone, A.; Prampolini, G. *Phys. Chem. Chem. Phys.* **2011**, *13*, 2160−2166.
(74) Biczysko, M.; Bloino, J.; Brancato, G.; Cacelli, I.; Cappelli, C.; Ferretti, A.; Lami, A.; Monti, S.; Pedone, A.; Prampolini, G.; Puzzarini, C.; Santoro, F.; Trani, F.; Villani, G. *Theor. Chem. Acc.* **2012**, *131*, 1−19.
(75) Bloino, J.; Biczysko, M.; Barone, V. *J. Chem. Theory Comput.* **2012**, *8*, 1015−1036.
(76) Wang, J. M.; Cieplak, P.; Kollman, P. A. *J. Comput. Chem.* **2000**, *21*, 1049−1074.
(77) Dixon, R. W.; Kollman, P. A. *J. Comput. Chem.* **1997**, *18*, 1632−1646.
(78) van der Spoel, D.; Lindahl, E.; Hess, B.; van Buuren, A. R.; Apol, E.; Meulenhoff, P. J.; Tieleman, D. P.; Sijbers, A. L. T. M.; Feenstra, K. A.; van Drunen R.; Berendsen, H. J. C. *GROMACS 4.5.4*, Gromacs User Manual version 4.5.4; 2010. www.gromacs.org (accessed Oct 11, 2012).
(79) Ruud, K.; Astrand, P.-O.; Taylor, P. R. *J. Chem. Phys.* **2000**, *112*, 2668−2683.
(80) Auer, A. A.; Gauss, J.; Stanton, J. F. *J. Chem. Phys.* **2003**, *118*, 10407−10417.
(81) Barone, V.; Improta, R.; Rega, N. *Acc. Chem. Res.* **2008**, *41*, 605−616.
(82) Puzzarini, C.; Barone, V. *Phys. Chem. Chem. Phys.* **2011**, *13*, 7189−7197.
(83) Rega, N.; Cossi, M.; Barone, V. *J. Am. Chem. Soc.* **1998**, *120*, 5723−5732.
(84) Hehre, W. J.; Ditchfield, R.; Pople, J. A. *J. Chem. Phys.* **1972**, *56*, 2257−2261.
(85) Krishnan, R.; Binkley, J. S.; Seeger, R.; Pople, J. A. *J. Chem. Phys.* **1980**, *72*, 650−654.
(86) Frisch, M. J.; Trucks, G. W.; Schlegel, H. B.; Scuseria, G. E.; Robb, M. A.; Cheeseman, J. R.; Scalmani, G.; Barone, V.; Mennucci,

B.; Petersson, G. A.; Nakatsuji, H.; Caricato, M.; Li, X.; Hratchian, H. P.; Izmaylov, A. F.; Bloino, J.; Zheng, G.; Sonnenberg, J. L.; Hada, M.; Ehara, M.; Toyota, K.; Fukuda, R.; Hasegawa, J.; Ishida, M.; Nakajima, T.; Honda, Y.; Kitao, O.; Nakai, H.; Vreven, T.; Montgomery, J. A., Jr.; Peralta, J. E.; Ogliaro, F.; Bearpark, M.; Heyd, J. J.; Brothers, E.; Kudin, K. N.; Staroverov, V. N.; Kobayashi, R.; Normand, J.; Raghavachari, K.; Rendell, A.; Burant, J. C.; Iyengar, S. S.; Tomasi, J.; Cossi, M.; Rega, N.; Millam, J. M.; Klene, M.; Knox, J. E.; Cross, J. B.; Bakken, V.; Adamo, C.; Jaramillo, J.; Gomperts, R.; Stratmann, R. E.; Yazyev, O.; Austin, A. J.; Cammi, R.; Pomelli, C.; Ochterski, J. W.; Martin, R. L.; Morokuma, K.; Zakrzewski, V. G.; Voth, G. A.; Salvador, P.; Dannenberg, J. J.; Dapprich, S.; Daniels, A. D.; Farkas, Ö.; Foresman, J. B.; Ortiz, J. V.; Cioslowski, J.; Fox, D. J. *Gaussian 09*, Revision A.02; Gaussian, Inc.: Wallingford, CT, 2009.

(87) Berendsen, H. J. C.; Postma, J. P. M.; van Gunsteren, W. F.; DiNola, A.; Haak, J. R. *J. Chem. Phys.* **1984**, *81*, 3684−3690.

(88) Darden, T.; York, D.; Pedersen, L. *J. Chem. Phys.* **1993**, *98*, 10089−10092.

(89) Essmann, U.; Perera, L.; Berkowitz, M. L.; Darden, T.; Lee, H.; Pedersen, L. G. *J. Chem. Phys.* **1995**, *103*, 8577−8593.

(90) Jorgensen, W. L.; Chandrasekhar, J.; Madura, J. D.; Impey, R. W.; Klein, M. L. *J. Chem. Phys.* **1983**, *79*, 926−935.

(91) Janzen, E. G.; Evans, C. A. *J. Am. Chem. Soc.* **1975**, *97*, 205−206.

(92) Makino, K.; Mossoba, M. M.; Riesz, P. *J. Am. Chem. Soc.* **1982**, *104*, 3537−3539.

(93) Symons, M. C. R.; Penanunez, A. S. *J. Chem. Soc., Faraday Trans. 1* **1985**, *81*, 2421−2435.